Characteristics of scalar dispersion in turbulent-channel flow

By Juan C. del Álamo † AND Javier Jiménez ‡

The dispersion of a passive scalar by wall turbulence, in the limit of infinite Peclét number, is analyzed using frozen velocity fields from the DNS of del Álamo & Jiménez (2001). The Lagrangian trajectories of fluid particles in these fields are integrated and used to compute the first- and second-order moments of the distribution of fluid-particle displacements. It is shown that the largest scales in the flow dominate turbulent diffusion, and the computed dispersion is in good agreement with measurements in the atmospheric boundary layer. This agreement can be understood by noting that the lifetimes of the large structures are much longer than the time scale of the transition from linear to Gaussian particle spreading in the cross-stream plane. Numerical experiments on computing the Lagrangian trajectories in reference frames moving at different velocities suggest that this transition is controlled by the difference between the mean streamwise velocity and the phase speed of the large-scale structures of the cross-stream velocity field. In the streamwise direction, the effect of the mean shear dominates and produces elongated scalar patches, with dispersion exponents which are different from the transverse ones.

1. Introduction

The prediction of diffusion characteristics in turbulent shear flows, particularly in those near walls, is a notoriously difficult problem. While, for example, the width of a contaminant plume follows a Gaussian spreading law relatively well in isotropic turbulence, or even in wall-bounded flows far enough from the source, this is not true closer to the source (Nokes & Wood 1988), near the wall, or in atmospheric flows. This is an important consideration in many practical applications, such as the prediction of dispersal of pollution from industrial plants, or of hazardous substances from either accidental or malicious releases. There are many other problems in which this subject is important, apart from the ones already mentioned. For instance, the diffusion of odors in the atmosphere is known to affect the migrational patterns of some insects, and it is not known whether similar effects occur in other anisotropic flows, such as near-surface ocean turbulence, where it could influence the rate of decay of the thermal wake of vehicles. The solution to these problems is typically estimated using empirical laws (Brown *et al.* 1997), or computed from semi-empirical models (Hanna *et al.* 1999). Many of these models are used for regulatory purposes, and the fact that some of them produce different results for the same input data is an indication of the difficulty of the problem. This has led to the development of standardization programs (Olesen 1995) with the purpose of establishing systematic procedures for the development and testing of dispersion models, based on compilations of meteorological data from field experiments. However, due to the inherent difficulty of performing such experiments, the data sets are scarce, the number

† School of Aeronautics UPM, 28040 Madrid, Spain.
‡ Also at School of Aeronautics UPM, 28040 Madrid, Spain.

Case	U_{adv}/U_b	Spatial Resolution	No. of Fields	No. of Particles per Field
1	0	full	1	2×10^5
2	0.84	full	1	2×10^5
3	0	$\lambda_x,\, \lambda_z > 0.25\,h$	3	2×10^5
4	0.84	$\lambda_x,\, \lambda_z > 0.25\,h$	3	2×10^5

TABLE 1. Summary of computed cases.

of measured magnitudes is limited, and some of the data sets are of doubtful accuracy (Olesen 1994).

Since the atmospheric effects are observed over scales of hundreds of meters, and there are sound theoretical reasons to expect small-scale turbulence to produce Gaussian diffusion at such long distances, it is tempting to conclude that the reason for the anomalous spreading is the presence of very large anisotropic scales (VLAS) in turbulent wall flows. Recently we have performed a direct numerical simulation of turbulent channel flow at moderate Reynolds number, which we believe to be the first which has both a Reynolds number high enough to observe some scale separation and a computational domain large enough not to interfere with the dynamics of the largest scales. The present work, which used flow data from this simulation, is intended to be a first step in using direct numerical simulation in research on atmospheric dispersion, which might contribute to diminishing the current experimental uncertainties.

2. Computing dispersion from frozen fields

We will consider the release of a passive scalar into turbulent channel flow in the limit of infinite Peclét number $U_b h/D$ (here U_b is the bulk mean velocity in the channel, h is the channel half-width, and D is the kinematic diffusivity of the scalar). In that case the dispersion of the scalar is controlled by the Lagrangian trajectories $\mathbf{x}$ of the fluid elements that transport it, given by

$$\frac{\mathrm{d}\mathbf{x}}{\mathrm{dt}} = \mathbf{u}(\mathbf{x}(t), t). \tag{2.1}$$

The main difficulty of computing the Lagrangian trajectories of fluid particles lies in knowing the unsteady three-dimensional velocity field $\mathbf{u}(\mathbf{x}, \mathbf{t})$, which has to be computed from the continuity and Navier-Stokes equations, leading to a problem much more expensive than the integration of (2.1) itself. Due to the preliminary nature of this work, and in order to avoid the computational expense of integrating in time the Lagrangian trajectories coupled with the velocity field, we have decided to calculate the former using frozen velocity fields which were already available from the DNS of turbulent channel flow by del Álamo & Jiménez (2001). This simulation was performed at a Reynolds number $Re_\tau = 550$ based on the friction velocity u_τ and on the channel half-width h, and its most important characteristic is that the computational domain is large enough not to interfere with the largest scales in the flow, which will allow us to study their effect on the scalar dispersion. The size of the numerical box is $L_x \times L_y \times L_z = 8\pi h \times 2h \times 4\pi h$ in the streamwise, wall-normal and spanwise directions, respectively. In isotropic turbulence the frozen-field approximation would be reasonable for times much shorter than the char-

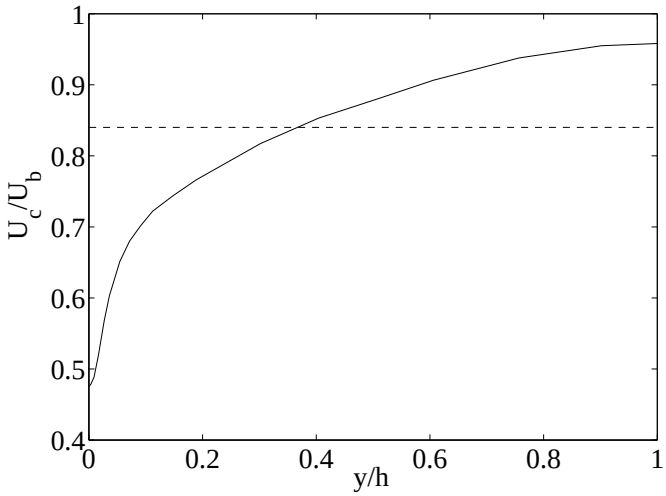

FIGURE 1. ——— , phase velocity U_c of the large-scale spanwise velocity component as a function of wall distance. Only structures such that $\lambda_x, \lambda_z \geq 0.25\,h$ are taken into account. ---- , advection velocity U_{adv} of the frozen fields.

acteristic lifetime of the eddies, which is proportional to their turnover time. However, this might not be true in wall turbulence, where the flow features are known to travel in the streamwise direction with an advection velocity of the order of U_b (Wills, 1964). This advection velocity, acting on scales of length λ, introduces a convective time scale $T_c \sim \lambda/U_b$ which is always shorter that the eddy-turnover time $T_L \sim \lambda/u_\tau$. We have tried to take into account the effect of the mean advection by integrating the Lagrangian trajectories from the frozen velocity fields in a moving reference frame,

$$\frac{d\mathbf{x}}{d\tau} = \mathbf{u}\left(\mathbf{x}(\tau) - \tau\mathbf{U_{adv}},\, t_0\right). \tag{2.2}$$

Here $\mathbf{u}(\mathbf{x}, \mathbf{t_0})$ is the instantaneous frozen velocity field at $t = t_0$, and $\mathbf{U_{adv}} = (U_{adv}, 0, 0)$ is the velocity of the reference frame, which can be interpreted physically as a choice for the convection or 'advection' velocity of the frozen fields. This choice affects the paths of fluid particles by modifying their velocities relative to the turbulent structures. In order to evaluate the effect of the convection velocity of the frozen fields in scalar dispersion, we have integrated (2.2) for two different values of U_{adv}. In one case we have chosen $U_{adv} = 0$, while in the other we have set it equal to the representative phase velocity of the large energetic scales in the flow, which have widths and lengths of the order of or larger than h (del Álamo & Jiménez 2001). There are several possible ways to compute the phase velocity of a flow variable (Wills, 1964; Hussain & Clark 1981; del Álamo & Jiménez 2002): this is the usual definition of convection velocity. Here we have computed it from the frequency-wavenumber power spectrum $P(\omega, k_x, y)$ as in Wills (1964), where the phase velocity is defined as the velocity $U_c(y)$ of the moving reference frame for which the integral time scale

$$T_L(k_x, y) = \frac{P(-U_c k_x, k_x, y)}{\int_{-\infty}^{\infty} P(\omega, k_x, y)\mathrm{d}\omega} \tag{2.3}$$

is a maximum. The frequency-wavenumber power spectrum has been computed using time histories of velocity fields that were available from the DNS, as was done by Choi

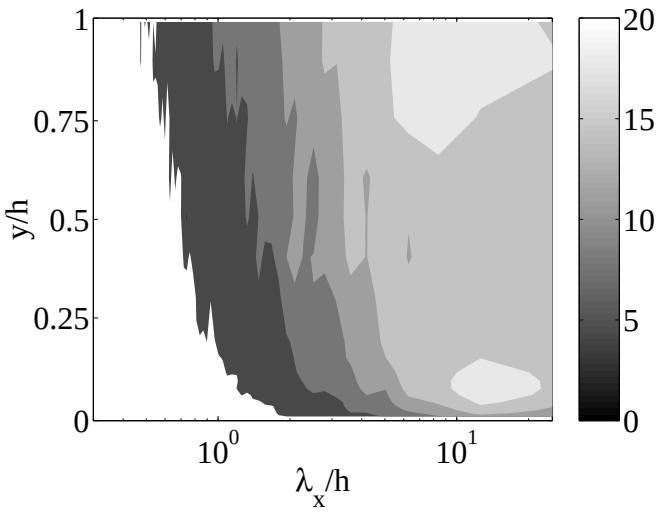

FIGURE 2. Lagrangian time scale $U_b T_L/h$ of the spanwise velocity, low-pass filtered in z ($\lambda_z > 0.25\,h$), as a function of the streamwise wavelength λ_x and wall distance y.

& Moin (1990). In the present case, the minimum and maximum frequencies imposed by the temporal sampling are $\omega_{min} = 0.14\,U_b/h$ and $\omega_{max} = 71\,U_b/h$. Due to storage limitations, the time histories of the velocity field were spatially filtered by removing all the length scales either shorter or narrower than $0.25\,h$ using a Fourier cut-off filter. Figure 1 displays the average phase speed of the low-pass-filtered spanwise-velocity fluctuations as a function of wall distance, and non-dimensionalized with the bulk mean velocity U_b (solid line), together with its average across the channel width (dashed line)

$$U_{adv} = \frac{1}{2h}\int_0^{2h} U_c(y)\mathrm{dy} = 0.84\,\mathrm{U_b}.$$

We have chosen this value as the advection velocity of the frozen fields to be used in (2.2) for our second set of numerical experiments. Kim & Hussain (1993) computed the propagation speeds of several turbulent magnitudes, including the velocity components, in a fully-resolved $Re_\tau = 180$ channel. They obtained a phase velocity of w in the near-wall region approximately equal to $10\,u_\tau$, which is the same as we have measured in the low-pass-filtered $Re_\tau = 550$ channel. In the outer region, however, they obtain convection velocities approximately 10% higher than we do, and which are closer to the local mean velocity in their case than in ours. This is not surprising. If we believe that turbulent structures propagate roughly at the average streamwise velocity that they feel, then the smaller scales should follow the local mean velocity better than the large ones.

The integral time scale T_L in (2.3) measures the characteristic time associated to the turbulent fluctuations of a given magnitude with a certain length $\lambda_x = 2\pi/k_x$ at a given wall-distance, and in a reference frame moving with their local advection velocity. This magnitude can be interpreted as the Lagrangian time scale seen by an observer following the mean trajectories of the eddies or, in other words, as the typical lifetime of the structures of a given length. The Lagrangian time scale of the fluctuations of spanwise velocity has been represented in figure 2, low-pass filtered in z, as a function of streamwise wavelength λ_x and wall distance y. The figure shows that the lifetimes of the large scales of w can be very long, even comparable to a 'wash-out' or 'through-flow' time $8\pi\,h/U_b$.

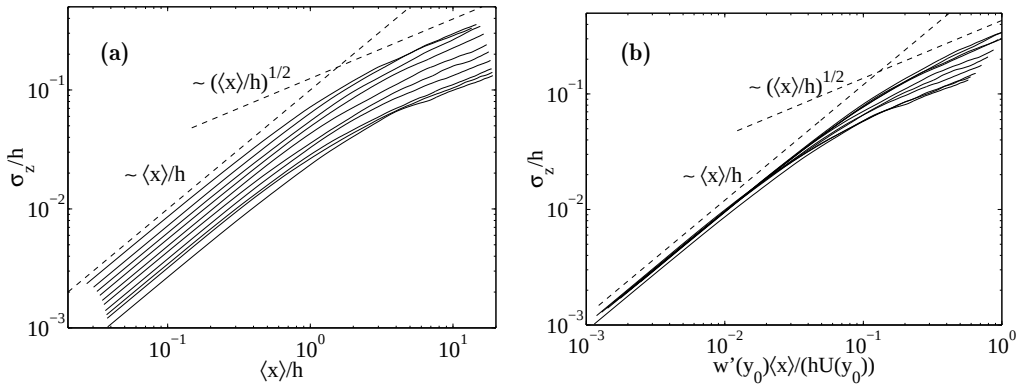

FIGURE 3. R.m.s. of the spanwise displacement σ_z of fluid particles as a function of their mean streamwise displacement $\langle x \rangle$. The different curves correspond to $y_0/h = 0.1(0.1)1$ from bottom to top. The dashed lines have logarithmic slopes 1 and 1/2. (a), using h as the scale of σ_z and $\langle x \rangle$; (b), using $w'(y_0)t$ as the scale of σ_z and $U(y_0)t$ as the scale of $\langle x \rangle$.

The values of T_L for the other two components of velocity, not shown here, are similar, and give an *a priori* estimate of the longest intervals of time for which we can expect the integration of (2.2) to provide reasonably accurate results. Note that this prediction would only be true if the large scales controlled the characteristics of dispersion. In order to analyze their importance in this phenomenon, we have solved (2.2) using both fully-resolved and low-pass-filtered fields. Overall, we have integrated (2.2) in four different cases, depending on the choice of U_{adv} and of the spatial resolution. These cases have been summarized in table 1, indicating the number of different fields that have been used for each case, as well as the number of trajectories that have been computed per field. The time discretization is fourth-order Runge-Kutta, and third-order B-splines have been used to interpolate the velocity field from the collocation points of the DNS.

3. Results. One-point statistics

The single-particle statistics $\langle x_i \rangle$ and $\sigma_i = \langle (x_i - \langle x_i \rangle)^2 \rangle^{1/2}$ are of great interest because they indicate respectively the mean displacement of the center of a typical scalar patch and its size in the three spatial directions, and also because the latter is often measured as a function of the former in field experiments, which will allow us to test the approximation (2.2). These magnitudes are functions of the initial position y_0 of the fluid element, of its instantaneous position y, and of time. Operating on (2.1) it is possible to obtain (Hunt 1985) that

$$\partial_t \sigma_i^2 = u_i'(y) u_i'(y_0) \int_0^t \rho_{ii}(r_x - \tau U_{adv}, r_z, y_0, y, t - \tau) \mathrm{d}\tau, \tag{3.1}$$

where ρ_{ii} is the two-point autocorrelation coefficient of the ith-component of the velocity vector. This magnitude is a function of the streamwise and spanwise separations r_x and r_z, of the initial and instantaneous wall distances, and of time. Note that the frozen-field approximation is equivalent to setting $t - \tau = 0$ in ρ_{ii} in (3.1). For times and spatial separations short compared with the corresponding integral scales, the velocity field is almost fully correlated, $\rho_{ii} \approx 1$, and $y_0 \approx y$. We then have

$$\sigma_i \approx u_i'(y_0) t \sim \langle x \rangle \approx U(y_0) t. \tag{3.2}$$

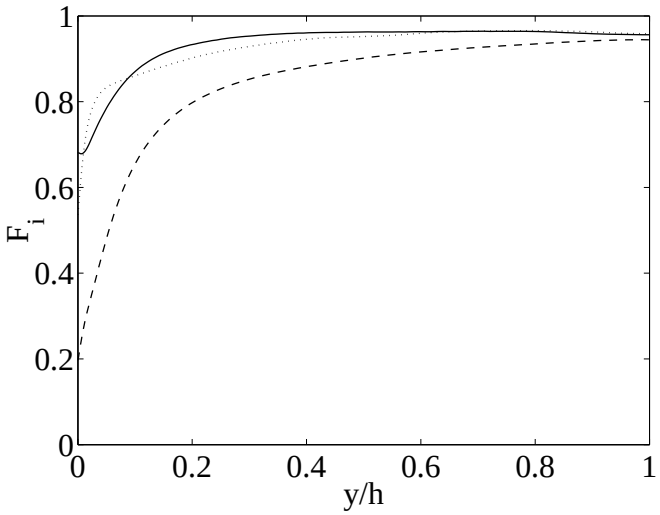

FIGURE 4. Fraction F_i of the ith-contribution to turbulent kinetic energy contained in the cut-off filtered fields as a function of wall-distance. ——— , u; - - - - , v; ····· , w.

On the other hand, for very long temporal and spatial separations the velocity field is approximately decorrelated, $\rho_{ii} \approx 0$, and the integral on the right-hand side of (3.1) is roughly independent of its upper limit. We then obtain the Gaussian spreading law $\sigma_i \sim (\langle x \rangle h)^{1/2}$. Both asymptotic behaviors can be observed in figure 3, where the solid curves show σ_z from case 2 as a function of the mean streamwise displacement for ten equispaced intervals of initial wall distance, from the wall to the center of the channel. In figure 3(a) we have used the channel half-width as the length scale for σ_z and $\langle x \rangle$, while in figure 3(b) we have scaled σ_z with $w'(y_0)t$ and $\langle x \rangle$ with $U(y_0)t$. The figures show that in the short-range limit, the curves representing σ_z are parallel to the dashed line with logarithmic slope 1, while far away from the release point the curves are roughly parallel to the dashed line with logarithmic slope 1/2. It can be observed in figure 3(b) that the scaling (3.2) gives a good collapse of the plume widths corresponding to different release points, at least at short distances from the source. As expected, the collapse worsens beyond the turning point in the curves, where their slope starts decreasing and (3.2) is no longer valid. The characteristic position of this turning point is a measure of the shortest integral scale involved in the dispersion process.

Equation (3.1) also suggests that the large scales may play an important role in turbulent dispersion. Coherent structures with $\lambda_x/h > 2$ and $\lambda_z/h \approx 1 - 2$ are known to be correlated right across the channel half-width and to contain a large fraction of the turbulent kinetic energy (del Álamo & Jiménez 2002), which suggests that they should contribute substantially to the right-hand side of (3.1). Figure 4 displays the fraction F of the total streamwise (solid line), wall-normal (dashed line) and spanwise (dotted line) contributions to kinetic energy contained in the cut-off filtered fields, as a function of wall distance. The figure shows that the structures which are longer and wider than $0.25\,h$ contain most of the kinetic-energy contributions of u and w in the outer region of the flow, and hence could be expected to produce values of σ_x and σ_z similar to the ones generated by the full fields. On the other hand, the small scales of v contain relatively more kinetic energy than those of u and w, suggesting that the value of σ_y computed from the filtered fields will be less accurate than that obtained from the full fields. This

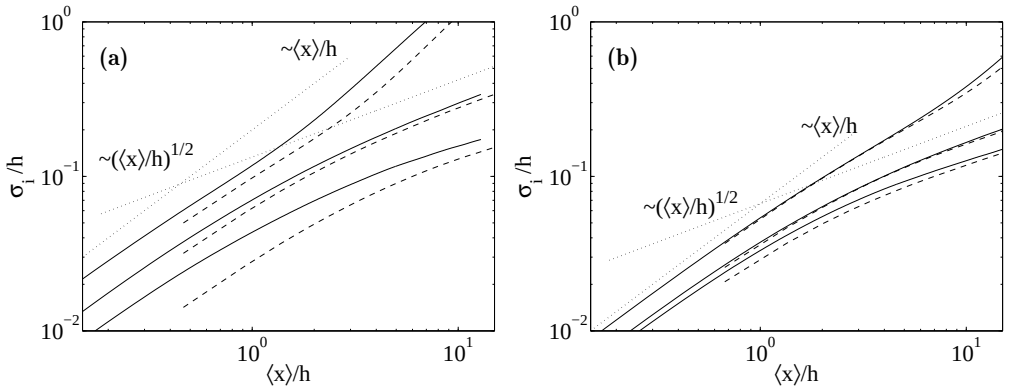

FIGURE 5. R.m.s. of the displacement of fluid particles in the ith-direction as a function of their mean streamwise displacement $\langle x \rangle$. Top, σ_x; middle, σ_z; bottom, σ_y. ——— , full DNS fields (case 2); - - - - , cut-off filtered DNS fields (case 4). In all the cases $U_{adv} = 0.84\,U_b$. (a), $y_0^+ < 100$; (b), $0.2 < y_0/h < 1$.

is actually what is observed in figure 5, where we have plotted the three components of σ (from top to bottom σ_x, σ_z and σ_y) computed from the full (case 2, solid lines) and the filtered (case 4, dashed lines) moving frozen DNS fields. In figure 5(a) the patch size has been averaged for fluid particles released in the near-wall region ($y_0^+ < 100$), while in figure 5(b) the average has been performed for initial positions in the outer region ($0.2 < y_0/h < 1$). The results from the filtered fields compare fairly well with those from the fully resolved ones in the outer region, while they underestimate the different components of the r.m.s. in the near-wall region. Note that the agreement between the different sets of data is better wherever F is higher, and *vice versa*, supporting the argument above. These observations agree with the previous work of Armenio *et al.* (1999), who performed a similar analysis using time-evolving velocity fields, with application to LES modeling. The results from the stationary frozen DNS fields (cases 1 and 3), not shown here, behave in the same way as those we have presented in figure 5.

Note that the standard deviations in figure 5 are always much smaller than $\langle x \rangle$, implying that the basic motion of the particles is advection by the local mean velocity, $\langle r_x \rangle \approx U(y_0)\tau$, while the spreading around that position is slow.

Figure 5 also shows the relative magnitudes of σ along the different axes, which give an idea of the evolution of the shape of a typical scalar patch with distance from the source. In the short-range region the three standard deviations grow at the same rate, and a typical cloud of scalar would initially conserve its original shape as it moved away from the release point. However, after the cloud has traveled a certain distance it would start elongating very rapidly, as we can deduce from the increase in the slope of σ_x that takes place at large distances, seen in the figure. Comparison of figures 5(a) and 5(b) indicates that this phenomenon occurs at a smaller distance from the source for lower values of y_0, and this is more apparent in figure 6. This figure displays the logarithmic slope of σ_x (from case 2) as a function of time for ten equispaced intervals of y_0. The slope of σ_x increases and reaches a maximum value after times which are longer as the curves move from the left to the right, corresponding to increasing values of y_0. There are strong reasons for believing that this effect is due to the mean shear. Scaling the time with $\partial_y U$, as in figure 6(b), collapses the position of the maxima of the different curves, indicating

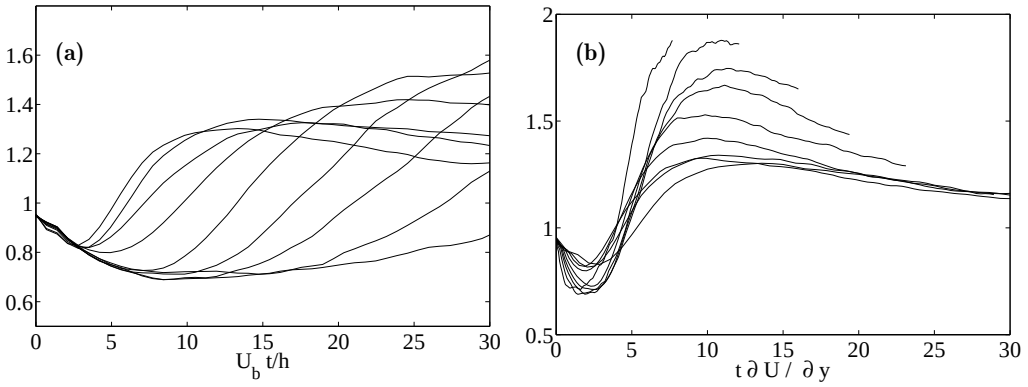

FIGURE 6. Logarithmic slope of σ_x (case 2) as a function of time t for $y_0/h = 0.1(0.1)1$. (a), using time non-dimensionalized with U_b/h. The curves peak at longer times as we move away from the wall; (b), using time non-dimensionalized with $\partial_y U$. The values of the maxima increase as we move away from the wall.

that the time scale associated with this phenomenon is the inverse of the mean shear. Also, in a different numerical experiment, we integrated (2.2) using fields from which we had removed the mean velocity profile, and the resulting σ_x behaved in the same way as σ_y and σ_z, without the transient increase in slope. Tennekes & Lumley (1972) show that in a flow subjected to a uniform shear S, the dispersion in the streamwise direction increases asymptotically with time as $(St)^{3/2}$. This value of the logarithmic slope lies roughly in the center of the set of different maximum values that we obtained from the DNS fields, and the scatter in the numerical values might be explained by the fact that $\partial_y U$ is not uniform in a turbulent channel.

3.1. *Comparison with atmospheric data*

In section 2 we discussed the *a priori* validity of our study, obtaining a rough estimate of the longest time intervals for which we could expect reasonable results from the model problem (2.2). Here we analyze the frozen-turbulence approximation *a posteriori*, by comparing the computed dispersion characteristics with those measured in the atmospheric boundary layer. Figure 7 shows the r.m.s. spanwise displacement of fluid particles as a function of their mean streamwise displacement. The symbols come from field experiments, most of which were compiled by Nielsen *et al.* (2002) and Olesen (1995). The atmospheric data sets are difficult to compare among themselves and with the numerical results. In general, the experiments consist of releasing a passive tracer from a smokestack and measuring its near-ground concentration along arcs situated at increasing distances from the release point. However, neither the releases nor the measurements were performed at the same ground distances in the different experiments; the monitoring procedures also differed, and so did the topological and meteorological conditions. Thus, any quantitative conclusion from the observations of figure 7 should be taken only as a guideline, as is also suggested by the scatter of the data in the figure. The solid line comes from our numerical results with $U_{adv} = 0.84\,U_b$, while the dashed line corresponds to $U_{adv} = 0$. In both cases we have represented the average values over the interval of particle positions $y/h < 0.1$, in order to compare with the atmospheric near-ground measurements. It should be noted however, that the numerical results contain the contributions from particles released at all possible wall distances across the

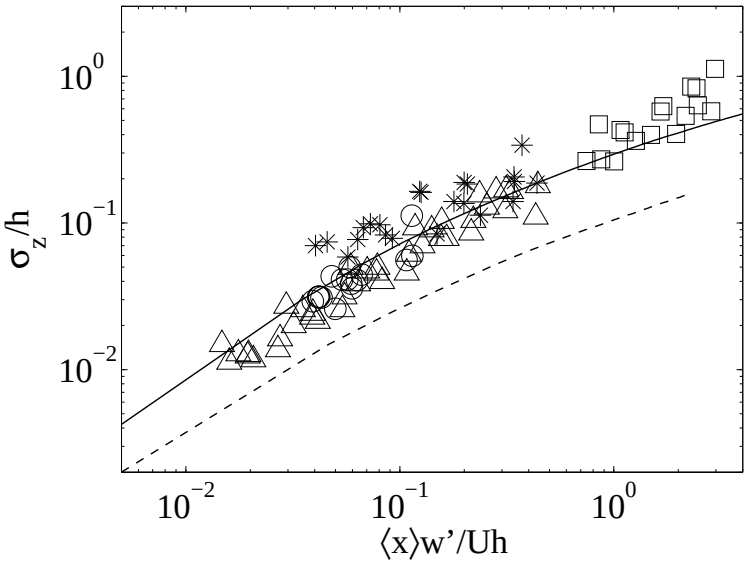

FIGURE 7. R.m.s. of the spanwise displacement of fluid particles, σ_z/h, as a function of their mean streamwise displacement $\langle x\rangle w'/(Uh)$. Lines, data from DNS fields; ——— , $U_{adv} = 0.84\,U_b$; - - - - , $U_{adv} = 0$. Symbols, atmospheric experiments; ∘, Ecofin Project (Nielsen *et al.* 2002); △ , Prairie Grass (Olesen 1995); ∗, Lillestrøm; ▫ , Copenhagen (Olesen 1995).

channel, while in the experiments the particles were released at a single distance above the ground. Even so, the agreement between the numerical and the experimental results is reasonably good for the results from the moving fields. They somewhat underestimate σ_z at large streamwise distances, but this could be because the atmospheric data in the corresponding experiment (the Copenhagen data set, represented by squares) were taken under unstably-stratified atmospheric conditions, with Monin-Obukhov lengths of the order of -100 m (Olesen 1994). The results from the stationary fields look qualitatively correct, but they predict widths smaller than the experimental values. This is understandable considering that, since the particles move approximately with the mean flow velocity, the mean streamwise separation that enters the correlation function in (3.1) is $\langle r_x\rangle \approx U(y_0)\tau$, so that the first argument in the autocorrelation coefficient of w is

$$\langle r_x\rangle - \tau U_{adv} \approx (U(y_0) - U_{adv})\tau.$$

In the stationary fields, fluid elements separate faster from their initial positions with respect to the flow structures than in the moving fields, because the difference between the mean velocity and that of the reference frame is higher in the former than in the latter. This is true all across the channel, except in the near-wall region where $U(y_0)$ is small. The fluid particles in the stationary 'snapshots' therefore feel a less-correlated velocity field than in the advecting cases, leading to lower values of σ_z. This argument is supported by figure 8, which shows the logarithmic slope of σ_z as a function of time (figure 8 (a)) and as a function of $|\langle r_x\rangle - \tau U_{adv}|$ (figure 8(b)), for five equispaced intervals of y_0 from the wall to the center of the channel. In figure 8(a) the logarithmic slope of σ_z decreases faster with time for the stationary fields (case 1), plotted with dotted lines, than for the moving ones (case 2), represented by solid lines. On the other hand, the curves in figure 8 (b) collapse fairly well, except for the curve on the left-hand side of

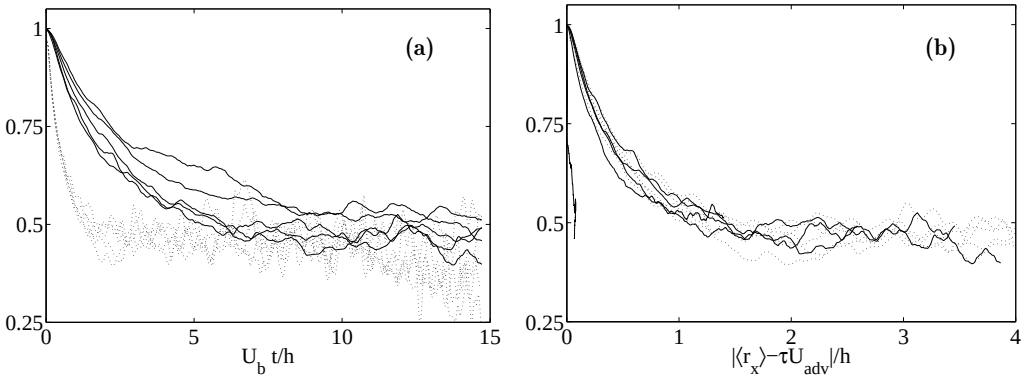

FIGURE 8. Logarithmic slope of σ_z for $y_0/h = 0.2(0.2)1$. (a), as a function of time $U_b t/h$. (b), as a function of the separation $|\langle r_x \rangle - \tau U_{adv}|/h$. ——— , $U_{adv} = 0.84\,U_b$. - - - - , $U_{adv} = 0$. The solid line that does not collapse well in the left-hand side of (b) corresponds to $y_0 = 0.2\,h$, near the critical layer at $y_c = 0.23\,h$;

the plot which corresponds to $y_0/h = 0.2$. This position is near the critical layer at $y_c = 0.23\,h$, where $U(y_c) = U_{adv}$. In that region, the mechanism that we have just described is weaker, and it is reasonable to think that the dispersion is dominated by the turbulent velocity fluctuations and not by the mean advection. Note that in the case of the stationary fields the critical layer is located at the walls, which may explain why all the dotted lines collapse well in figure 8(b). The behavior that we have observed in figure 8 is common to the results from both the fully-resolved and the cut-off filtered fields.

As we have mentioned, the location of the point where the logarithmic slopes of $\sigma_{y,z}$ decay from 1 to their asymptotic value of 1/2 is a measure of the integral scale most relevant to turbulent dispersion in the cross-stream plane. The fact that the results from the moving frozen fields, which neglect the time evolution of turbulent structures, are able to predict the position of the turning region in the data from the field experiments, can help us identify that integral scale. The large scales of w have lifetimes (see figure 2) which are approximately 4 times longer than the time scale of to the decay of the slope of σ_z from the moving fields (figure 8(a)). This suggests that the temporal decay of the turbulent structures may not be important in the decorrelation that the particles feel as they move in the flow. On the other hand, the streamwise separation corresponding to the transition of σ_z shown in figure 8(b), is $r_x \approx h$. This length is essentially equal to the position of the peak of the premultiplied energy spectrum of w (del Álamo & Jiménez 2001), which is a measure of its streamwise integral scale. These observations also apply to the wall-normal direction, for which the experimental information is much scarcer than for the spanwise direction. They suggest that the transition in $\sigma_{y,z}$ may be caused by the difference between the mean velocity of the flow, and the phase speed of the velocity components in the cross-stream plane.

4. Conclusions

The results show that the large scales of turbulent channel flow play a very important role in turbulent dispersion in the outer region of the flow, especially in the streamwise and spanwise directions. These structures contain a large fraction of the turbulent kinetic energy, and they are correlated across the full channel (del Álamo & Jiménez 2002), so

they are expected to contribute substantially to the standard deviations in (3.1). Filtered velocity fields, retaining only structures with λ_x, $\lambda_z > 0.25\,h$, produce more than 90% of $\sigma_{x,z}$ and roughly 80% of σ_y in the outer region. These results indicate that LES should be a valuable tool in the study of scalar dispersion.

The transition from linear to Gaussian spreading is due to the decorrelation of the velocity field along the Lagrangian trajectories of the particles. The lifetimes of the large scales of the spanwise velocity are roughly four times longer than the time scale of the decay in the slope of the plume width from 1 to 1/2. Thus, the time evolution of turbulent structures does not seem to be significant in the decorrelation process that leads to Gaussian spreading and, to a first approximation, it may be possible to study turbulent diffusion using frozen velocity fields. In fact, we have integrated the Lagrangian trajectories of fluid particles from frozen velocity fields, obtaining values of σ_z that agree well with atmospheric measurements. The agreement is better when the trajectories are computed in a reference frame moving with the average phase velocity of the large scales. The stationary frozen fields, on the other hand, produce values of σ_z smaller than those from the field experiments. This is because the decorrelation times experienced by the fluid elements in the stationary fields are shorter than those in the moving ones. In both cases, the decay in the slope of σ_z takes place when the streamwise separation of the particles relative to the velocity fields, $\langle r_x \rangle - \tau U_{adv}$, is roughly equal to the streamwise integral scale of w. Since the particles move in the x direction approximately following the mean velocity profile, their separation with respect to their initial positions is given by $(U(y_0) - U_{adv})\tau$, suggesting that the main cause of the transition from linear to Gaussian spreading is the difference between the mean streamwise velocity and the phase speeds of the velocity components in the cross-stream plane.

The mean shear is the dominating mechanism in the streamwise direction. It generates values of σ_x much greater than σ_y or σ_z, and leads to very elongated patch shapes. Although this consideration is not important in the case of the dispersion of contaminants from a continuous source, it may be fundamental in the case of discrete releases.

Acknowledgements

This work was supported by grant BFM 2000-1468 of CICYT. J.C.A. was supported by the CTR and by the Spanish Ministry of Education. The authors would like to thank Helge R. Olesen at NERI, Denmark for providing a digital version of the atmospheric data sets collected by the Harmonisation Group. We are also indebted to Julian C. R. Hunt, with whom we had fruitful discussions related to the subject of this work.

REFERENCES

Armenio, V., Piomelli, U. & Fiorotto, V. 1999 Effect of the subgrid scales on particle motion. *Phys. Fluids* **11**, 3030–3042.

Brown, M. J., Arya, S. P. & Snyder, W. H. 1997 Plume descriptors derived from a non-Gaussian concentration model. *Atmospheric Environment* **31**, 183–189.

Choi, H., Moin, P. 1990 On the space-time characteristics of wall-pressure fluctuations. *Phys. Fluids A* **2**, 1450–1460.

del Álamo, J. C. & Jiménez, J. 2001 Direct numerical simulation of the largest scales in a turbulent channel. *Annual Research Briefs*, Center for Turbulence Research,

NASA Ames/Stanford Univ., 329–341. Also in *Advances in Turbulence IX*, (Castro, I. P., Hancock, P. E. & Thomas, T. G., eds.) CIMNE, 403-406.

del Álamo, J. C. & Jiménez, J. 2002 The organization of the outer region of turbulent channels. *In preparation.*

Hanna, S. R., Egan, B. A., Purdum, J. & Wagler J. 1999 Evaluation of the ADMS, AERMOD and ISC3 Models with the Optex, Duke Forest, Kincaid, Indianapolis and Lovett Field Data Sets. *Proc. of Rouen Conference 11–14 October 1999.*

Hunt, J. C. R. 1985 Turbulent diffusion in complex flows. *Ann Rev. Fluid Mech.* **17**, 447–485.

Hussain, A. K. M. F. & Clark, A. R. 1981 Measurements of wavenumber-celerity spectrum in plane and axisymmetric jets. *AIAA J.* **19**, 51-55.

Kim, J. & Hussain, A. K. M. F. 1993 Propagation velocity of perturbations in turbulent channel flow. *Phys. Fluids A* **5**, 695–706.

Nielsen, M., Chatwin, P. C., Jørgensen, H. E., Mole, N., Munro, R. J. & Ott, S. 2002 Concentration Fluctuations in Gas Releases by Industrial Accidents. *RisøReport* **R-1329 (EN)**.

Nokes, R. I. & Wood, I. R. 1988 Vertical and lateral turbulent dispersion: some experimental results. *J. Fluid Mech.* **187**, 373–394.

Olesen, H. R. 1994 Model Validation Kit for the workshop on Operational Atmospheric Dispersion Models for Environmental Impact Assessments in Europe. *Report of the NERI, Denmark.*

Olesen, H. R. 1995 The model validation exercise at Mol: overview of results. *Int. J. Environment and Pollution* **5, Nos. 4–6**, 781–784.

Tennekes, H. & Lumley, J. L. 1972 *A First Course in Turbulence.* The MIT Press, p. 232.

Wills, J. A. B. 1964 On convection velocities in turbulent shear flows. *J. Fluid Mech.* **20**, 419–432.